Viser Technology Pte. Ltd.
Research and Application of Materials Science
DOI: 10.33142/rams.v7i1.18639

Research Article Open Access

High Performance N, C -Codoped $Na_3V_2(PO_4)_3$ Cathode Material for Sodium-ion Batteries

Jiayu LI*, Xiao FU

Public Experiment Center, University of Shanghai for Science and Technology, Shanghai, 200093, China

*Corresponding Author: Jiayu Li, E-mail: 249595941@qq.com

Abstract

A typical NASICON type cathode material, $Na_3V_2(PO_4)_3$ (NVP) has been widely studied in the field of sodium-ion batteries (SIBs), which possesses a suitable price, an ideal specific capacity, and an excellent cycling stability. However, its low ionic/electronic conductivity has become a major factor hindering its development. In the present study, carbon and nitrogen co-doped NVP (NVP/CN) composites are synthesized by adding $C_3N_6H_6$ source using a simple preparation method. The carbon and nitrogen co-doping is intended to introduce lattice defects, which enhances the electrical conductivity of the material and facilitates the diffusion of Na^+ and e^-. Comprehensively, the co-coated NVP cathode material show more excellent electrochemical performance when the N source addition of $nC_3N_6H_6$: nNVP=2 (NVP/CN-2). NVP/CN-2 has an initial discharge specific capacity of 111.5 mAh/g, and a capacity retention rate of 97.57% after 1000 charge/discharge cycles. The diffusion coefficient of sodium ions is relatively high and can reach 4.74×10-10 cm^2 s^{-1} by CV fitting, so the modified NVP/CN samples are expected to be promising cathode materials for sodium-ion batteries.

Keywords: *$Na_3V_2(PO_4)_3$; Modification; Sodium ion; Carbon-Nitrogen Co-Coating*

1 Introduction

Lithium-ion batteries, known for their high energy density, extended cycle life, and long-term usability, are currently widely applied in various fields such as portable power sources, electric vehicles, household appliances, smart wearable devices, and 3C products. They are also increasingly becoming the primary power source for new energy vehicles and energy storage, garnering significant attention in recent years[1-3]. However, as these Lithium-ion batteries are being utilized on a larger scale, cost and safety concerns are gaining prominence. Sodium-ion batteries (SIBs) hold promise as an alternative to lithium-ion batteries due to their cost-effectiveness and superior performance in high-low temperature environments [4-6]. Key factors determining the performance of sodium-ion battery cathode materials include the appropriate operating voltage, high reversible capacity, and structural stability[7]. A wide range of sodium-ion battery cathode materials have been reported, including layered and tunnel-type transition metal oxides, transition metal sulfides and fluorides, oxygen-containing anion compounds, Prussian blue analogs, and polymers[8-10]. However, due to the larger ionic radius of Na (1.02 Å) compared to Li (0.76 Å)[11], the sodium ion extraction process has implications for the stability, transport properties, and phase interconversion of material, resulting in suboptimal electrochemical performance[12-13].

Currently, cathode materials for sodium-ion batteries with the Na superionic conductor (NASICON) structure have garnered widespread attention[14-16]. These materials exhibit a three-dimensional open framework and larger interstitial channels, providing a theoretical basis for achieving rapid Na^+ transport[17-18]. One such material is NVP, which consists of VO_6 octahedral and PO_4 tetrahedral units. Sodium atoms reside in two distinct interstitial spaces and channels within the framework, creating two different oxygen environments[19]. This vanadium-based electrode exhibits two oxidation-reduction potentials at 3.4 V and 1.6 V, corresponding to the redox transitions of V^{3+}/V^{4+} and V^{2+}/V^{3+}. Notably, the 3.4 V flat plateau voltage is associated with a high theoretical capacity (117 mAh/g)[20]. To prevent the generation of V^{2+} during charge and discharge processes, voltage control is commonly employed to regulate electrochemical reactions, ensuring the reversibility of vanadium[21]. However, the intrinsic low electron conductivity of the material impacts its rate capability and cycling stability, mainly due to the relatively large atomic distances resulting from the independent VO_6 octahedral and PO_4 tetrahedral units that

Copyright © 2024 by author(s). This work is licensed under a Creative Commons Attribution-Noncommercial-No Derivative Works 4.0 License.
Received on March 20, 2025; Accepted on April 30, 2025

make up the NASICON-type framework[22].

Thus, to address the aforementioned challenges and enhance the cycling performance and rate capability of $Na_3V_2(PO_4)_3$ batteries, two primary strategies have emerged. The first involves improving the material's interfacial performance. This can be achieved through carbon coating to enhance surface conductivity, resulting in a reduction in surface resistance[23-25]. Additionally, the introduction of metal ions to generate electrons or vacancies can enhance conductivity[26-27]. The second strategy centers on controlling the diffusion distance of sodium ions within the material. This is accomplished by reducing particle size and fabricating specialized positive electrode materials with features like porosity or mesoporosity, effectively shortening the migration pathway and enabling rapid charge and discharge in the battery[28-29].

In this study, we employ a straightforward hydrothermal assisted sol-gel approach to synthesize $Na_3V_2(PO_4)_3$/C cathode materials. By means of surface carbon and nitrogen co-coating modification, it is intended to effectively improve the electrical conductivity of $Na_3V_2(PO_4)_3$ cathode materials. Additionally, we utilize NaOH, NH_4VO_3, and $NH_4H_2PO_4$ as raw materials, with ascorbic acid as a reducing agent and $C_3N_6H_6$ as a nitrogen source. By adjusting the quantity of $C_3N_6H_6$ added, we examine its multifaceted impact on the structure, morphology, and electrochemical performance of the composite material. The experiments reveale that when the $C_3N_6H_6$: NVP ratio is 2 (molar ratio, n:n), the material exhibited the better outstanding performance.

2 Experimental Section

2.1 Materials synthesis

$Na_3V_2(PO_4)_3$/CN composites were prepared by a previously reported hydrothermal route combined with a sol-gel method[30-31]. In a typical synthesis process, the measured $NH_3H_2PO_4$ was meticulously dissolved in a NaOH solution, resulting in solution A. Concurrently, NH_4VO_3 was dissolved in an ascorbic acid solution, creating solution B. A was then gently introduced into B, magnetic stirring at room temperature to ensure adequate mixing, after which the mixture was transferred to a 40 ml Teflon-lined autoclave, the solution was heated at 190 ℃ in a closed autoclave and kept for 36 hours, then cooling naturally to room temperature. The resulting brown mixture was ultrasonicated for 120 minutes to homogenize the dispersion. upon cooling to room temperature, the gel was subjected to additional heating and stirring in a constant-temperature water bath at 75 ℃. Following these steps, the gel was dried in a 60 ℃ oven under atmospheric conditions for 12 hours. Subsequently, the milled powder underwent further heat treatment in a nitrogen atmosphere at 350 ℃ for 4 hours, followed by an 8-hour calcination at 800 ℃, cooled to room temperature and then grounded again to obtain the final product $Na_3V_2(PO_4)_3$/CN-x, abbreviated as NVP/CN-x. The prepared NVP/CN-x was based on the ratios of the amount of $C_3N_6H_6$ added, n_{C3N6H6}: n_{NVP} = 1, 2, 3, 4 named NVP/CN-1, NVP/CN-2, NVP/CN-3, and NVP/CN-4, respectively. For comparison, NVP/C prepared by the same method without $C_3N_6H_6$ addition of raw material was the comparative sample.

2.2 Material characterizations and electrochemical measurements

The crystal structures of all samples were determined using X-ray diffraction (XRD, Rigaku, Japan) in the scanning range of 10 °～60 ° at a scanning speed of 4 °/min. Surface morphology of the electrode materials was analyzed by scanning electron microscopy (SEM, ZEISS, SUPRA-55). Electrochemical characterization of $Na_3V_2(PO_4)_3$ electrodes were investigated by a coin half-cell (CR2032) assembled in an argon glove box. A working electrode was made by doping 80 wt% of active material (NVP, cathode electrode material), 10 wt% of acetylene black (conductive agent) and 10 wt% of polyvinylidene difluoride binder (PVDF) into N-methyl-2-pyrrolidone (NMP). The resulting paste was pasted onto aluminium foil, then the final cathode electrode sheet was obtained by drying the electrodes in a vacuum at 120 ℃ for 8 h. The electrolyte consisted of ethylene carbonate (EC), dimethyl carbonate (DEC) and fluoroethylene carbonate (FEC) in 1 M $NaClO_4$, where the volume ratio of EC to DEC was 1:1 and FEC was 5 wt%. Glass fiber membrane (Whatman, GF/D) was used as the septum and sodium foil as the anode electrode. The charge/discharge performance was tested at room temperature (25 ℃) using a Land2001A system, and cyclic voltammetry (CV) tests were performed at different scan rates of 0.1 , 0.25, 0.5, and 1 mV s^{-1} in the range of 2.5～3.8 V (potential vs. Na/Na^+). Electrochemical impedance spectroscopy (EIS) measurements were performed in the frequency range of 10^{-1} Hz 10^5 Hz.

3 Results and Discussion

The XRD patterns of NVP/CN-x (x=1, 2, 3, 4) and NVP/C are shown in Figure 1, and they can be indexed to the rhombohedral NASICON structure with space group R3c (PDF standard card #00-62-0345)[32]. It belongs to the hexagonal crystal system, which is consistent with the previous reports, the diffraction peaks of the material are all relatively sharp, and the bottom back of the diffractogram is flat, indicating that good crystallinity of the material, and the XRD pattern shows the absence of heterogeneous peaks, which demonstrates that the purity of the substance is very high. It's worth noting that due to the nitrogen and carbon formation are amorphous, there is no effect on the structure of $Na_3V_2(PO_4)_3$/CN, therefore no diffraction peaks associated with carbon and nitrogen[33]. The peak

intensity of the diffraction peaks while decreasing slightly with the rise in $C_3N_6H_6$ doping is due to the increase in amorphous material and the decrease in crystalline $Na_3V_2(PO_4)_3$ content, which leads to a decrease in crystallinity.

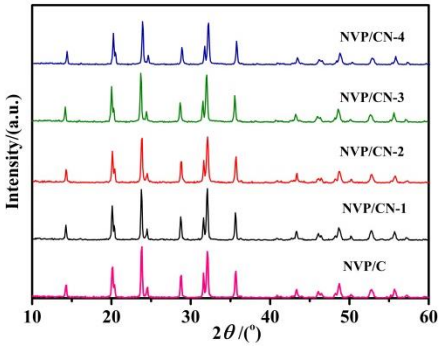

Figure 1 XRD patterns NVP/CN-x (x=1, 2, 3, 4) and NVP/C samples

The morphological features of NVP/CN-x (x=1, 2, 3, 4) composites with varying carbon and nitrogen content are described in Figure 2. From the figure, it can be observed that some fine particles obviously exist on the surface of NVP/CN-x (x=1, 2, 3, 4) particles, and with the increase of carbon and nitrogen content, the particle size of the surface particles of the NVP/CN-x (x=1, 2, 3, 4) composites decreases, and the particle size distribution tends to be more uniform. However, the aggregation of surface particles tends to be more serious with the continuous increase of carbon and nitrogen content, which is the same as that of simple carbon coating, the presence of moderate amount of carbon and nitrogen content can well prevent the growth of particles[34], and the increase of nitrogen content can also make the particle surface too thickly coated, or even bonded, which is unfavorable to the migration of sodium ions. The elemental analysis revealed that the carbon and nitrogen content in the four NVP/CN-x (x=1, 2, 3, 4) composite materials was 6.1wt%, 8.2wt%, 9.9wt%, and 12.0wt%, respectively.

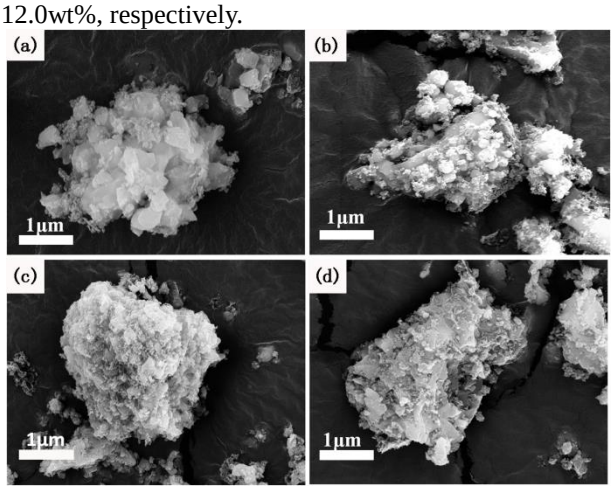

Figure 2 SEM images of NVP-x samples: (a) NVP/CN-1, (b) NVP/CN-2, (c) NVP/CN-3, (d) NVP/CN-4

Figure 3 illustrates the initial charge/discharge curves of NVP/C and NVP/CN-x (x=1, 2, 3, 4) samples obtained at a 0.2 C rate within the voltage range of 2.5～3.8 V (vs. Na^+/Na). As depicted, all samples exhibit prolonged and distinct voltage plateaus. The plateau at 3.4 V (vs. Na^+/Na) corresponds to the reversible phase transition between $Na_3V_2(PO_4)_3$ and $NaV_2(PO_4)_3$. Notably, NVP/CN-2 demonstrates the highest discharge capacity (111.5 mAh/g) and exhibits the narrowest plateau gap between charge and discharge curves, indicative of superior redox kinetics. Due to the different electronegativity between the carbon and nitrogen elements, doping of nitrogen leads to the formation of an n-type matrix. The multi-electron character of nitrogen alters the original electronic balance, generating additional active sites and enhancing electronic conductivity.

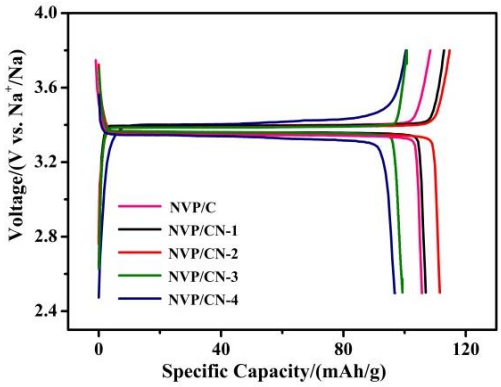

Figure 3 The initial charge-discharge curves of NVP/CN-x (x=1, 2, 3, 4) and NVP/C samples

The rate performance of NVP/C and NVP/CN-x (x=1, 2, 3, 4) composite materials is presented in Figure 4 The electrodes are successively charge and discharge 10 times at each of the 0.2 C～ 20 C rates, and return to the initial rate (0.2 C) after 70 cycles of charge and discharge. Corresponding to the initial charge-discharge cycle, NVP/CN-2 exhibits the better rate performance. It delivers discharge capacities of 111.4, 106.1, 101.4, 97.6, 93.9, 90.5, and 85.0 mAh/g at rates of 0.2 C, 0.5 C, 1 C, 2 C, 5 C, 10 C, and 20 C, respectively. Surprisingly, after undergoing 70 cycles at different rates, the discharge capacity of NVP/CN-2 can recover to 111.2 mAh/g (a retention rate of 99.82%) when the rate is reduced back to 0.2 C. It demonstrates the excellent reversibility of sodium storage. Furthermore, it's observed that NVP/CN-2 exhibits a noticeable enhancement in electrochemical performance compared to NVP/C, particularly at high rates such as 20 C. This enhancement is attributed to the nitrogen doping, which generates more defects in the original carbon layer, facilitating the migration of large sodium ions and aiding in sodium ion diffusion. Conversely, as the carbon and nitrogen content increases further, the rate performance of NVP/CN-x materials deteriorates. It may be due to excessive carbon

and nitrogen content leading to a reduction in the energy density of the cathode material, as well as the encapsulation of the active material, which hinders sodium ion diffusion, collectively resulting in a decline in electrochemical performance[35]. Proper carbon-nitrogen doping contributes to the improvement of the rate performance of material.

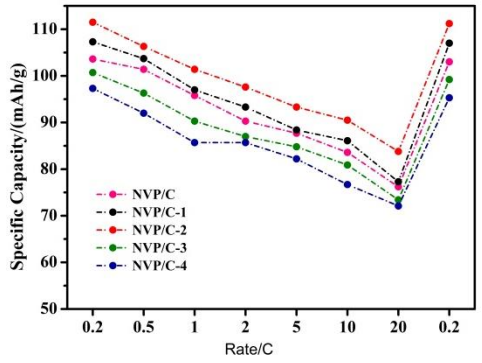

Figure 4 Rate performance of NVP/CN-x (x=1, 2, 3, 4) and NVP/C

Figure 5 illustrates the long-term cycling performance of NVP/CN-x (x=1, 2, 3, 4) and NVP/C samples at a 0.2 C rate. As shown, the retention rates after 1000 cycles for NVP/C and NVP/CN-x are as follows: 80.68%, 97.57%, 96.68%, 90.94%, and 70.45%. Notably, NVP/CN-2 and NVP/CN-3 exhibit the better cycling performance. These experimental findings suggest that defects induced by the nitrogen doping in the carbon layer are advantageous for enhancing electronic conductivity and improving interfacial charge transfer, thereby enhancing cycling stability[36]. However, as the nitrogen content increases, excessive surface defects in the material lead to extensive contact with the electrolyte, resulting in increased side reactions and severe polarization.

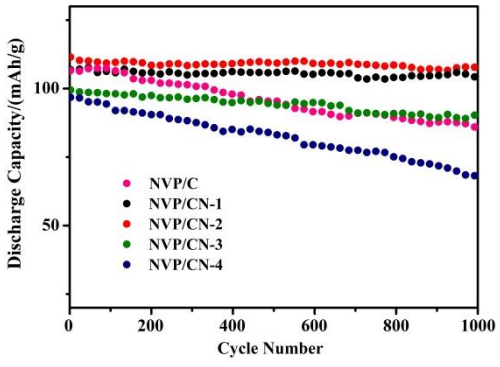

Figure 5 Cycle performance of NVP/CN-x (x=1, 2, 3, 4) and NVP/C

In order to further investigate the electrochemical processes, cyclic voltammetry (CV) tests are performed on NVP/CN-x (x = 1, 2, 3, 4) and NVP/C cathode materials. Cyclic voltammetry tests are performed between 2.5 and 3.8 V at a scan rate of 0.1 - 1 mV/s. All electrodes exhibit a pair of redox peaks at 3.4 V at different scan rates attributed to V^{3+}/V^{4+} redox reactions.[37-38] Figures 6 a and 6 c depict the cyclic voltammetry (CV) curves of NVP/CN-2 and NVP/C samples at scan rates of 0.1, 0.25, 0.5, and 1 mV/s. It is evident that with increasing scan rates, the both samples exhibit higher polarization. In comparison, the oxidation-reduction peaks of NVP/CN-2 are more symmetric and sharp, indicating better reversibility. The Na^+ diffusion coefficients were calculated using the classical Randles-Sevcik equation[39]:

$$I_p = 2.69\times10^5 n^{3/2} S D_{Na}^{1/2} v^{1/2} C_0 \quad (1)$$

Here, I_p represents the peak current (A), n denotes the number of electron transfers, S represents the area of the active material on the electrode, D_{Na} stands for the sodium ion diffusion coefficient, v represents the scan rate, and C_0 represents the concentration of sodium ions in the electrode. Figure 6b displays the linear fit of peak current (I_p) and the square root of the scan rate ($v^{1/2}$). Based on Equation (1), sodium ion diffusion coefficients can be obtained by the slope of the fitted line. The diffusion coefficients for the positive and anode electrodes of NVP/CN-2 are 4.74×10^{-10} and 3.98×10^{-10} $cm^2\ s^{-1}$, respectively, while the corresponding diffusion coefficients of NVP/C are 9.65×10^{-11} and 9.32×10^{-11} $cm^2\ s^{-1}$, demonstrating superior performance compared to previously reported diffusion coefficients[40].

EIS is used to evaluate the kinetic characteristics of NVP/CN-x (x = 1, 2, 3, 4) electrode materials. Measurements are performed in the range of 10^{-1} Hz to 10^5 Hz prior to charging and discharging. The spectra of all samples consist of a semicircle in the high-frequency region and a tilted straight line in the low-frequency region. The semicircle observed in the high-frequency range of the Nyquist plot is attributed to charge transfer resistance (R_{ct}) and the diagonal line in the low frequency region corresponds to the Warburg impedance. The R_{ct} of NVP/C and NVP/CN-x (x = 1, 2, 3, 4) are 380.01, 321.13, 289.16, 534.58, and 626.46 Ω, respectively. Evidently, with the increase of carbon and nitrogen content, the R_{ct} value shows a decreasing and then increasing trend, in which NVP/CN-2 exhibits a lower R_{ct} compared to NVP/C and other coated samples, it is demonstrated that the NVP/CN-2 cathode material possesses a faster charge transfer rate, which is consistent with the previous test results. This is attributable to the fact that the carbon and nitrogen coating enhances the electronic conductivity of the particle surface and increases the electronic contact between the particles, which reduces the charge transfer impedance, but as the carbon and nitrogen content is excessively increased, the platelet adhesion occurs on the surface of the material, which is unfavorable to the charge transfer of the material. It is shown that appropriate nitrogen element doped carbon coatings can promote charge transfer and obtain excellent electrochemical properties.

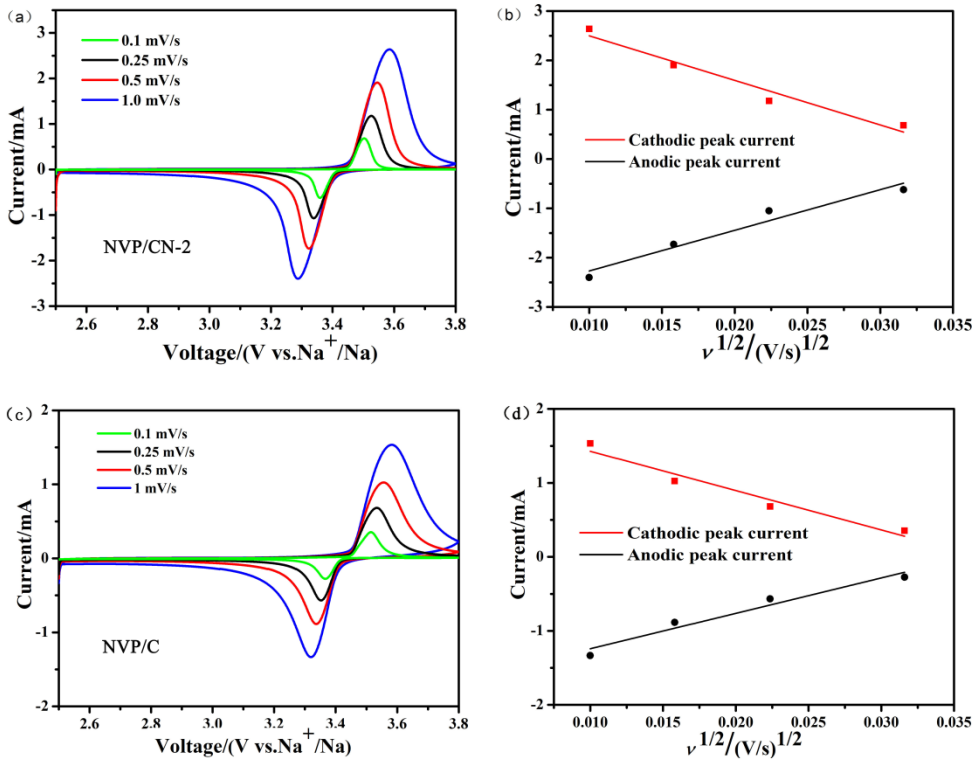

Figure 6 CV curve of NVP/CN-2 and NVP/CN samples in 2.5-3.8 V voltage : (a)(c) At different scanning speeds, (b)(d) The relationship of I_p vs $v^{1/2}$

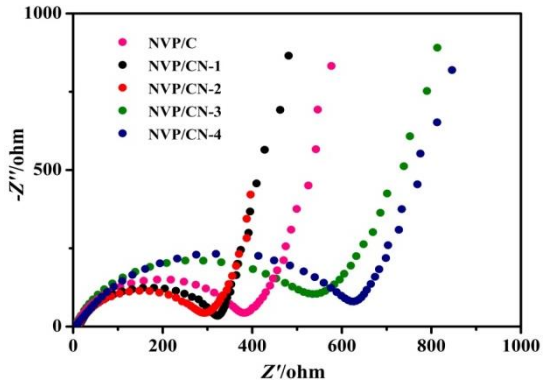

Figure 7 Nyquist plots of NVP/CN-x (x=1, 2, 3, 4) and NVP/C samples

4 Conclusion

This study explored the impact of controlled nitrogen doping in the form of nitrogen -doped carbon layers on $Na_3V_2(PO_4)_3$/C composite materials. The electronic conductivity of the composites is enhanced because the doped nitrogen provides electrons to the carbon matrix. A series of electrochemical tests also demonstrat that an appropriate amount of nitrogen doping plays an important role in the electrochemical performance of the $Na_3V_2(PO_4)_3$/C electrode. When the nitrogen source ($C_3N_6H_6$), is added with an NVP:$C_3N_6H_6$ molar ratio of 2, the discharge capacity reached 111.5 mAh/g. Even after cycling (70 cycle numbers) at various rates (0.2 C to 20 C), the capacity could be restored to 111.2 mAh/g when the rate was reduced back to 0.2 C, with a remarkable retention rate of 99.82%. These results show outstanding cycling performance. The judicious introduction of nitrogen element yields an appropriate number of surface defects, reducing charge transfer resistance, increasing conductivity between particles, and facilitating electron transfer, ultimately resulting in exceptional electrochemical performance.

These authors contributed equally to this work.

References

[1] Wu W W, Sun Z G, He Q, et al. Boosting Lithium-Ion Transport Kinetics by Increasing the Local Lithium-Ion Concentration Gradient in Composite Anodes of Lithium-Ion Batteries [J]. ACS Applied Materials and Interfaces, 2021(13):14752-14758.

[2] Duffner F, Kronemeyer N, Jens T, et al. Post-lithium-ion battery cell production and its compatibility with lithium-ion cell production infrastructure [J]. Nature Energy, 2021(6):123-134.

[3] Pender, J P, Jha G, Youn H, et al. Electrode Degradation in Lithium-Ion Batteries [J]. ACS Nano, 2020(14):1243-1295.

[4] Zhao Y, Kang Y Q, Wozny J, et al. Recycling of sodium-ion batteries [J]. Nature Reviews Materials, 2023(8):623-634.

[5] Yang Z, Li G, Sun J, et al. High performance cathode material based on $Na_3V_2(PO_4)_2F_3$ and $Na_3V_2(PO_4)_3$ for sodium-ion batteries [J]. Energy Storage Materials, 2020(25):724-730.

[6] Klein F, Jache B, Bhide A , et al. Conversion reactions for sodium-ion batteries [J]. Physical Chemistry Chemical Physics, 2023(15):15876-15887.

[7] Philipp A, Pascal H, Bender C L, et al. From lithium to sodium: cell chemistry of room temperature sodium-air and sodium-sulfur batteries [J]. Beilstein J Nanotechnol, 2015(6):1016-1055.

[8] Chen J W, Adi G, Li L, et al. Optimization Strategies Toward Functional Sodium-Ion Batteries [J]. Energy & Environmental Materials, 2023(6):4.

[9] Shi C H, Wang L G, Chen X, et al. Challenges of layer-structured cathodes for sodium-ion batteries [J]. Nanoscale Horizons, 2022(7):338-351.

[10] Xiao J, Li X, Tang K K, et al. Recent progress of emerging cathode materials for sodium ion batteries [J]. Materials Chemistry frontiers, 2021(5):3735-3764.

[11] Li L, Zheng Y, Zhang S L, et al. Recent progress on sodium ion batteries: potential high-performance anodes [J]. Energy & Environmental Science, 2018(11):2310-2340.

[12] Jiang Y, Yang Z, Li W, et al. Nanoconfined Carbon-Coated $Na_3V_2(PO_4)_3$ Particles in Mesoporous Carbon Enabling Ultralong Cycle Life for Sodium-Ion Batteries [J]. Advanced Energy Materials, 2015(5):1402104.

[13] Hwang J Y, Myung S T, Sun Y K. Sodium-ion batteries: present and future [J]. Chemical Society Reviews, 2017(46):3529-3614.

[14] Wu Y C, Meng X H, Yan L J, et al. Vanadium-free NASICON-type electrode materials for sodium-ion batteries [J]. Journal of Materials Chemistry A, 2022(10):21816-21837.

[15] Chen S Q, Wu C, Shen L F, et al. Challenges and Perspectives for NASICON-Type Electrode Materials for Advanced Sodium-Ion Batteries [J]. Advanced Materials, 2017(29):1700431.

[16] Singh K, Chakraborty A, Thirupathi R, et al. Recent advances in NASICON-type oxide electrolytes for solid-state sodium-ion rechargeable batteries [J]. Ionics, 2022(28):5289-5319.

[17] Cheng J, Chen Y, Sun S, et al. $Na_3V_2(PO_4)_3$/C·$Na_3V_2(PO_4)_2F_3$/C@rGO blended cathode material with elevated energy density for sodium ion batteries [J]. Ceramics International, 2021(47):18065-18074.

[18] Salehi A H, Masoudpanah S M, Hasheminiasari M, et al. A solution synthesis of $Na_3V_2(PO_4)_3$ cathode for sodium storage by using CTAB additive [J]. Solid State Ionics, 2020(347):115269.

[19] Jian Z, Zhao L, Pan H, et al. Carbon coated $Na_3V_2(PO_4)_3$, as novel electrode material for sodium ion batteries [J]. Electrochemistry Communications, 2012(14):86-89.

[20] Jiang X M, Liu C C, Tian Z Y, et al. Constructing p-type substitution induced by Ca^{2+} in defective $Na_3V^{2-}xCax(PO_4)_3$/C wrapped with conductive CNTs for high-performance sodium-ion batteries [J]. Dalton Transactions, 2022(51):16145-16157.

[21] Lim S Y, Kim H, Shakoor R A, et al. Electrochemical and Thermal Properties of NASICON Structured $Na_3V_2(PO_4)_3$ as a Sodium Rechargeable Battery Cathode: A Combined Experimental and Theoretical Study [J]. Journal of the Electrochemical Society, 2013(159):A1393-A1397.

[22] Kang J, Baek S, Mathew V, et al. High rate performance of a Na3V2(PO4)3/C cathode prepared by pyro-synthesis for sodium-ion batteries [J]. Journal of Materials Chemistry, 2012(22):20857-20860.

[23] Chen L, Zhao Y, Liu S H, et al. Hard carbon wrapped $Na_3V_2(PO_4)_3$@C porous composite extending cycling lifespan for sodium-ion batteries [J]. ACS Applied Materials and Interfaces, 2017(9):44485-44493.

[24] Chen H, Huang Y, Mao G, et al. Reduced graphene oxide decorated $Na_3V_2(PO_4)_3$ microspheres as cathode material with advanced sodium storage performance [J]. Frontiers in Chemistry, 2018(6):174.

[25] Jiang Y, Zhou X, Li D, et al. Highly Reversible Na Storage in $Na_3V_2(PO_4)_3$ by Optimizing Nanostructure and Rational Surface Engineering [J]. Advanced Energy Materials, 2018(8):1800068.

[26] Wang X X, Wang W W, Zhu B C, et al. Mo-doped $Na_3V_2(PO_4)$3@C composites for high stable sodium ion battery cathode [J]. Frontiers of Materials Science, 2018(12):53-63.

[27] Chen Y J, Xu Y L, Sun X F, et al. Effect of Al substitution on the enhanced electrochemical performance and strong structure stability of $Na_3V_2(PO_4)_3$/C composite cathode for sodium-ion batteries [J]. Journal of Power Sources, 2018(375):82-92.

[28] Ruan Y L, Liu J J, Song S D, et al. Multi-hierarchical nanosheet-assembled chrysanthemum-structured $Na_3V_2(PO_4)_3$/C as electrode materials for high-performance sodium-ion batteries [J]. Ionics, 2018(24):1663-1673.

[29] Zhao Y L, Cao X X, Fang G Z, et al. Hierarchically carbon-coated $Na_3V_2(PO_4)_3$, nanoflakes for high-rate capability and ultralong cycle-life sodium ion batteries [J]. Chemical Engineering Journal, 2018(339):162-169.

[30] Duan W C, Zhu Z Q, Li H, et al. $Na_3V2(PO_4)_3$@C core-shell nanocomposites for rechargeable sodium-ion batteries [J]. Journal Of Materials Chemistry A, 2014(2):8668-8675.

[31] Sun Q, Chen Y J, Tian Z Y, et al. Biomimetic synthesis of craspedia globosa-shaped $Na_3V2(PO_4)_3$ with high performance for sodium ion batteries [J]. Journal of Alloys And Compounds, 2022(909):164719.

[32] Hu F, Jiang X. A stable and superior performance of $Na_3V_2(PO_4)_3$/C nanocomposites as cathode for sodium-ion batteries [J]. Inorganic Chemistry Communications, 2020(115):107860.

[33] Liang X, Ou X, Zheng F, et al. Surface modification of $Na_3V_2(PO_4)_3$ by nitrogen and sulfur dual-doped carbon layer with advanced sodium storage property [J]. ACS Applied Materials & Interfaces, 2017(9):13151-13162.

[34] Zuo P, Cheng G, Wang T, et al. Effects of Carbon on Structure and Electrochemical Performance of Li_2FeSiO_4

Cathode materials for lithium-ion batteries [J]. RSC Advances, 2012(2):6994-6998.

[35] Zhuo H, Wang X, Tang A, et al. The preparation of NaV^{1-} $xCrxPO_4F$ cathode materials for sodium-ion battery [J]. Journal of Power Sources, 2006(160):698-703.

[36] M. Hankel, D. Ye, L. Wang, D.J. Searles, Lithium and sodium storage on graphitic carbon nitride [J], Journal of Physical Chemistry C, 2015(119):21921-21927.

[37] Jiang Y, Zhang H C, Yang H, et al. $Na_3V_2(PO_4)_3$@nitrogen,sulfur-codoped 3D porous carbon enabling ultra-long cycle life sodium-ion batteries [J]. Nanoscale, 2017(9):6048-6055.

[38] Li X M, Wang S J, Tang X, Porous $Na_3V_2(PO_4)_3$ nanoplates for high-performance sodium storage [J]. JournaL of Colloid And Interface Science, 2019(539):168-174.

[39] Du K, Guo H, Hu G, et al. $Na_3V_2(PO_4)_3$ as cathode material for hybrid lithium ion batteries [J]. Journal of Power Sources, 2013(223):284-288.

[40] Luo S H, Li J Y, Bao S, et al. $Na_3V_2(PO_4)_3$/C composite prepared by sol-gel method as cathode for sodium ion batteries [J]. Journal of the Electrochemical Society, 2018(165):A1460-A1465.